Quaternary Science Reviews 70 (2013) 63–72

Contents lists available at SciVerse ScienceDirect

Quaternary Science Reviews

journal homepage: www.elsevier.com/locate/quascirev

Quantitative assessment of glacial fluctuations in the level of Lake Lisan, Dead Sea rift

Eelco J. Rohling [a,b,*]

[a] Research School of Earth Sciences, The Australian National University, Canberra, ACT 0200, Australia
[b] School of Ocean and Earth Science, University of Southampton, National Oceanography Centre, Southampton SO14 3ZH, UK

ARTICLE INFO

Article history:
Received 24 September 2012
Received in revised form
1 March 2013
Accepted 22 March 2013
Available online

Keywords:
Lake Lisan
Quantitative climate reconstruction
Precipitation
Evaporation
Wind speed

ABSTRACT

A quantitative understanding of climatic variations in the Levant during the last glacial cycle is needed to support archaeologists in assessing the drivers behind hominin migrations and cultural developments in this key region at the intersection between Africa and Europe. It will also foster a better understanding of the region's natural variability as context to projections of modern climate change. Detailed documentation of variations in the level of Lake Lisan – the lake that occupied the Dead Sea rift during the last glacial cycle – provides crucial climatic information for this region. Existing reconstructions suggest that Lake Lisan highstands during cold intervals of the last glacial cycle represent relatively humid conditions in the region, but these interpretations have remained predominantly qualitative. Here, I evaluate realistic ranges of the key climatological parameters that controlled lake level, based on the observed timing and amplitudes of lake-level variability. I infer that a mean precipitation rate over the wider catchment area of about 500 mm y^{-1}, as proposed in the literature, would be consistent with observed lake levels if there was a concomitant 15–50% increase in wind speed during cold glacial stadials. This lends quantitative support to previous inferences of a notable increase in the intensity of Mediterranean (winter) storms during glacial periods, which tracked eastward into the Levant. In contrast to highstands during 'regular' stadials, lake level dropped during Heinrich Events. I demonstrate that this likely indicates a further intensification of the winds during those times.

1. Introduction

The Levant is located at the intersection between Africa and Europe, and is one of a few prime routes for hominin migrations and cultural exchanges between these continents (e.g., Fernandes et al., 2006; Abbate and Sagri, 2012; and references therein). Archaeologists require a detailed and well-dated understanding of climatic variations in the region in order to assess the potential role of climate in driving or facilitating hominin migrations and cultural developments.

Implications for hominins are not the only reason for striving toward a better understanding of Levantine climate variability. Parts of the region are highly sensitive to potential aridification under global climate change (e.g., Watson et al., 1997), and future projections require a sound understanding of any underlying natural variability. Similarly, intensive anthropogenic water use (e.g., diversion of the Jordan River) and proposed engineering projects such as a Red Sea–Dead Sea canal are presenting unprecedented challenges to the environment, assessment of which may be helped by a better understanding of the region's natural variability (for evaluations of these contemporaneous issues, see for example: Salhotra et al., 1985; Stanhill, 1994; Alpert et al., 1997; Asmar and Ergenzinger, 2002a,b,c,d; 2003; Lensky et al., 2005).

The present paper focuses on natural variability during the last glacial cycle (specifically, the last 120,000 years). A recent overview (Frumkin et al., 2011), which extends on previous syntheses (e.g., Enzel et al., 2003, 2008), offers a comprehensive overview of climatic changes in the Levant based on varied evidence. This included changes in the level, sedimentology, and chemical properties of Lake Lisan (Fig. 1), cave speleothem deposits, and loess deposits in the region. In particular, reconstructions indicate a similarity between Lake Lisan level fluctuations and Northern Hemisphere climate 'cycles' as recorded in Greenland ice-core records (among many others: Bartov et al., 2002; Migowski et al., 2006; Stein and Goldstein, 2006; Waldmann et al., 2007, 2010; Lisker et al., 2009; Torfstein et al., 2009, 2013a; and Stein, Goldstein, and Enzel, pers. comm. at the Ein Gedi fieldtrip, 2012). Early work

* Research School of Earth Sciences, The Australian National University, Canberra, ACT 0200, Australia.
E-mail address: eelco.rohling@anu.edu.au.

0277-3791/$ – see front matter © 2013 Elsevier Ltd. All rights reserved.
http://dx.doi.org/10.1016/j.quascirev.2013.03.013

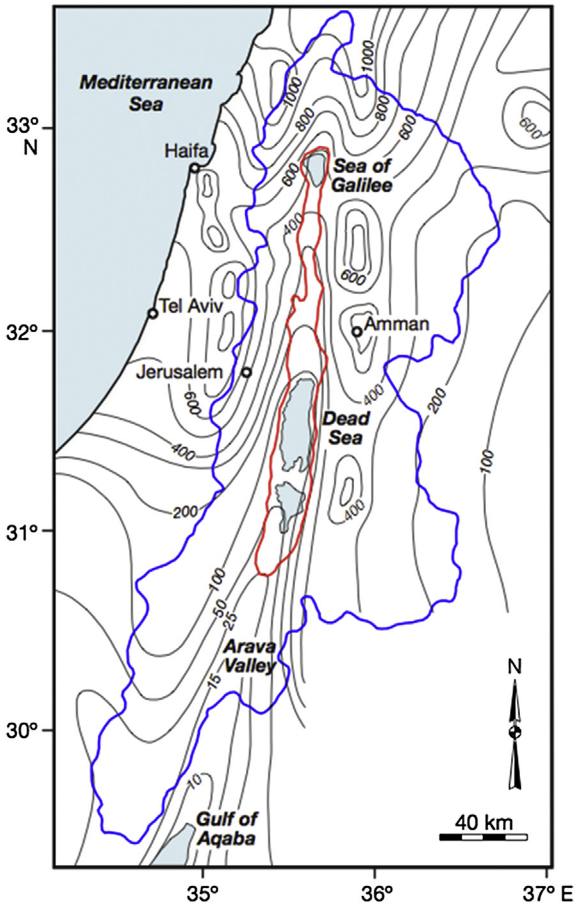

Fig. 1. Map of the Levant, with annual mean isohyets (in mm y^{-1}). The red line outlines the maximum size of Lake Lisan, and the blue line outlines the Dead Sea/Lake Lisan catchment area. Modified after Waldmann et al. (2010), with additional catchment data from FAO GEONETWORK (2010).

had suggested that cold episodes in Greenland correlated with arid conditions in the Levant on decadal to centennial timescales (e.g., Prasad et al., 2004). However, the detailed studies listed above comprehensively demonstrate that cold episodes were instead associated with Lake Lisan highstands on multi-centennial to millennial timescales, reaching up to 200 m or more above the modern Dead Sea level. Intervals corresponding to Heinrich events appear to have deviated from that pattern, with dry conditions and relative lowstands in Lake Lisan (although still 60–120 m above the present-day Dead Sea level; Bartov et al., 2003; Torfstein et al., 2013a).

The previous work generally argued that Lake Lisan highstands represent climatically wet episodes. To date, however, such interpretations have remained largely phenomenological, did not really account for variability in the (large) evaporative loss term, and were expressed in qualitative or semi-quantitative terms only. The present study builds on this previous work and on modelling of recent changes in the region (Salhotra et al., 1985; Stanhill, 1994; Alpert et al., 1997; Asmar and Ergenzinger, 2002a,b,c,d; 2003; Lensky et al., 2005), to advance a quantitatively coherent understanding of relationships between the various observed aspects of regional climate variability over the last glacial cycle. A basic model is developed in which lake level depends on changes in evaporation from the variable Lake Lisan surface area, and on mean net precipitation over the wider catchment area. I then evaluate – for observed timings and amplitudes of lake-level variations – realistic precipitation ranges over the wider catchment, given values (with uncertainties) of evaporation fluctuations that are based on realistic ranges of variability in key climatological parameters. The solutions provide internally consistent suites of potential variability in the regional climate (precipitation, evaporation, wind speed) and lake level over the last glacial cycle. The model is not exhaustive and lacks details that are included in the aforementioned studies of recent changes, which is deliberate to make it applicable to the long timescales and large uncertainties (shortage of direct measurements) associated with geological studies. Despite these simplifications, the results provide indicative, internally consistent, first-order estimates of regional environmental variability.

2. Method

As with any lake, fluctuations in the level of Lake Lisan (H) reflect the integration over time of mean net precipitation (Ψ) over the lake's wider catchment area (A_{catch}), and evaporation (E) from the lake's surface area (A). The lake's surface area varies with its level; as lake level rises, the lake occupies more of the rift valley, and its surface area increases (Fig. 1). This variation of surface area with lake level is important, because the rate of evaporation, which affects the lake surface area, is high in this region. Currently, the rate of evaporation from fresh water (often referred to as 'pan evaporation') is of the order of -3 m y^{-1} in this region (Alpert et al., 1997). Due to the influences of high salinity (around $S = 276$), however, the rate of evaporation from the sea itself is near to -1.3 m y^{-1} (note, these are pre-1951 values that pre-date extensive anthropogenic diversion of the Jordan River) (Salhotra et al., 1985; Stanhill, 1994; Alpert et al., 1997). In contrast to A, the size of A_{catch} (which receives the precipitation that feeds the lake) is determined by the larger-scale regional topographic configuration, which is assumed to have remained constant throughout the last glacial cycle (Fig. 1).

Today, A_{catch} is roughly 40 times larger than the Dead Sea surface area (e.g., Waldmann et al., 2010; Frumkin et al., 2011) (Fig. 1). To maintain the Dead Sea at steady state, water gain from mean net precipitation (Ψ_{mod}) over the catchment must balance the evaporative water loss (-1.3 m y^{-1}) over the Dead Sea surface area ($A_{DS_{mod}}$). Rapid responses of the Dead Sea level to modern droughts demonstrate that this steady state response is not greatly delayed by groundwater inertia (Enzel et al., 2003), which agrees with experiments that reveal high groundwater flow rates (Magal et al., 2010). Hence, Ψ_{mod} over A_{catch} in this steady state scenario needs to be of the order of 1.3/40 m per year; i.e., 33 mm y^{-1}. Using the approximation given in Frumkin et al. (2011) for modern mean gross precipitation (P_{mod}), which is $P_{mod} = \Psi_{mod}/0.3$, P_{mod} is estimated at 110 mm y^{-1}, where the difference between P_{mod} and Ψ_{mod} is due to evaporation and evapotranspiration. The value of 110 mm y^{-1} determined here for mean annual precipitation over the lake's catchment area compares well with the rainfall distribution compilations of Enzel et al. (2003, 2008), Waldmann et al. (2010) and Frumkin et al. (2011) (Fig. 1).

Evaporation from a freshwater body predominantly depends on surface-water and air temperature (and, therefore, on the lake-air temperature difference), relative humidity, and wind stress. Here I adapt the calculations of Rohling (1999) to the Dead Sea/Lake Lisan configuration. In that formulation, evaporation from low-salinity waters (in m y^{-1}) is given by:

$$E_{lowS} = -\rho_a LCV(q_s - rq_a)1.26 \times 10^{-2} \quad (1)$$

where ρ_a is the air density at mean lake-level pressure (set to 1012 mbar); $L = (2500.83 - 2.34T_s) \times 10^3$ is the latent heat of vapourisation in J kg^{-1} at surface-water temperature T_s in °C (Abbott and Tabony, 1985); $C = 1.15 \times 10^{-3}$ is an exchange coefficient (Garrett et al., 1993; Wells, 1995); V is wind speed in m s^{-1}; r is relative humidity as a fraction between 0 and 1; q_s is the saturation vapour pressure at surface-water temperature T_s; and q_a is the saturation vapour pressure at air temperature T_a (measured at 10 m above the lake surface). Values for q are determined after Abbott and Tabony (1985) and Wells (1986) (for details, see Rohling, 1999).

For the Dead Sea/Lake Lisan situation, the influence of high salinity needs to be accounted for. It reduces the rate of evaporation relative to that determined for low-salinity water according to a factor $\alpha = E/E_{lowS}$ (Salhotra et al., 1985; Stanhill, 1994), which depends on density but can be sufficiently approximated for the problem studied here based on the dominating salinity dependence. Comparison of the values for α with salinity (S) in the experiments of Salhotra et al. (1985) gives a reasonable linear relationship of $\alpha = 1–0.0015\ S$ ($R^2 = 0.82$; $N = 8$; $48 \leq S \leq 278$).

Fluctuations in the level of Lake Lisan, with amplitudes of change of the order of 200 m, appear to have followed Northern Hemisphere climate variations (e.g., Bartov et al., 2003; Waldmann et al., 2010; Frumkin et al., 2011;). At the millennial scale, those variations are portrayed by the air-temperature dominated Dansgaard–Oeschger (D–O) cycles in Greenland ice-core δ^{18}O (Dansgaard et al., 1993; Grootes et al., 1993). Signal similarity to the D–O cycles has also been reported for a number of Mediterranean sea surface temperature records (e.g., Cacho et al., 1999, 2001, 2002; Sprovieri et al., 2003; Martrat et al., 2004, 2007; Frigola et al., 2008). Although the eastern Mediterranean climate is not likely to have exactly followed the D–O cycles, a suitable first-order experiment can be performed in which the lake-level model is driven with prescribed variations in air temperature T_a and lake surface-water temperature T_s that are assumed to be in direct proportion with D–O fluctuations in the NGRIP ice-core record (North Greenland Ice Core Project Members, 2004), using $T_a = T_{a(mod)} + f\Delta_{T_a}$ and $T_s = T_{s(mod)} + f\Delta_{T_s}$. Here ΔT_a and ΔT_s are single values that represent the total glacial-interglacial amplitudes of change in air and surface-water temperature imposed in each scenario, respectively, while $T_{a(mod)}$ and $T_{s(mod)}$ are each scenario's modern values. The parameter f is a non-dimensional scaling coefficient that imposes fluctuations in proportion with the D–O cycles: $f = (\delta_{NG} - \delta_{NGmod})/\delta_{NGrange}$ where δ_{NG} is the NGRIP δ^{18}O at each time step, δ_{NGmod} is the modern value (top of the record) and $\delta_{NGrange}$ is the total range between the minimum glacial value and δ_{NGmod}. Changes in mean net precipitation over the wider catchment area (Ψ, in m y^{-1}) are similarly considered, using $\Psi = (1 + fF_\Psi)\Psi_{mod}$. Here Ψ_{mod} is the modern value for each scenario, as determined by dividing the calculated E_{mod} for each scenario (i.e., $E_{lowS(mod)}$ from Equation (1), times α_{mod}) by the ratio between the wider catchment and modern Dead Sea surface areas (i.e., $\Psi_{mod} = -E_{mod}/40$). The term F_Ψ represents the total glacial-interglacial amplitude of precipitation change in fractional form; for example, $F_\Psi = +0.4$ would mean that maximum glacial Ψ was 40% greater than Ψ_{mod}.

Evaporation acts over the surface area of the lake. Changes in lake surface area are calculated as a function of lake level following a simple approximation, namely that $\varepsilon = A/A_{DSmod} \approx 1.25 + 0.025H$. Here the constant approximates the area of the Dead Sea before major anthropogenic diversion of the Jordan River (relative to that of the modern Dead Sea area) at which time the Dead Sea level stood above the threshold that separates the southern Dead Sea from the main basin (Stanhill, 1994). A is the surface area of past Lake Lisan, A_{DSmod} is that of the modern Dead Sea, and H is the height of the past Lake Lisan level in m relative to the southern Dead Sea threshold at about 10 m above the current level. The applied relationship follows a geometric ratio within the rift topography as estimated from topographic sections of Wdowinski and Zilberman (1997). Salinities are determined by volumetric dilution of the present-day Dead Sea salinity (about 330), using lake-level dependent volume changes based on a triangular basin morphology. With a present-day mean Dead Sea depth of 118 m, relative changes in volume (Ω) are approximated by $\eta = \Omega/\Omega_{DSmod} = 1 + 0.5\varepsilon H/118$. The salinity effect on evaporation is determined using the relationship for α described above. Although the geographic approximations used here may certainly be refined using digital elevation models and hydro-isostatic modelling, the scale of such refinements remains secondary to the large uncertainties in the climatic factors that underlie lake-level changes in the geological past. Therefore, simple geographic approximations suffice for this study's objective of a first quantitative exploration of the Lake Lisan variations through time.

Past values of E are calculated by multiplying α (a function of S) with E_{lowS} from Equation (1), which uses the temporally varying climate parameters described above. These results are then used to determine bi-decadal (20-year) steady states between E, Ψ, and the evolving H, S, and A, relative to a constant value for A_{catch}. Solutions are determined by iteratively optimising F_Ψ so that the maximum (centennial-scale averaged) lake-level within the last glacial cycle reaches $H = 200$ m, in approximation of observations. Finally, the difference term Δ_Ψ (in m y^{-1}; $\Delta_\Psi = \Psi - \Psi_{mod}$) represents the change in mean net precipitation over the lake catchment. It comprises a component of change in gross precipitation (Δ_P), as well as a component of change in evaporation over the catchment region (Δ_E, where it must be noted that this depends on the area-weighted mean of E_{lowS} over the catchment region outside Lake Lisan, and αE_{lowS} over Lake Lisan); $\Delta_\Psi = \Delta_P + \Delta_E$. Hence, the change in precipitation can be evaluated using $\Delta_P = \Delta_\Psi - \Delta_E$. Besides Δ_P and Δ_E, relative to the present, the solutions are expressed in absolute values of P and E by adding each scenario's Δ_P and Δ_E values to each scenario's P_{mod} and E_{mod} (about 110 mm y^{-1} and -1.3 m y^{-1}, respectively). The entire sequence of calculations is summarised in a flowchart (Fig. 2), and a summary of key parameters is given in Appendix I.

Experiments were conducted over a range of scenarios. Values for Δ_V are considered between -1 and 2.5 m s^{-1} (the range within which realistic solutions exist in which lake level reaches +200 m). The inter-related terms Δ_{T_a} and Δ_{T_s} are varied together, within realistic constraints to their ratio ($\Delta_{T_a}/\Delta_{T_s}$). Given that land temperature changes are on average about 1.5 × larger than marine temperature changes (Brannocot et al., 2007, 2012), that Lake Lisan has less thermal inertia than the open sea, and that lake and overlying air temperatures ultimately are strongly related, the range considered is $1.0 \leq \Delta_{T_a}/\Delta_{T_s} \leq 1.5$. Estimates for Δ_{T_a} are obtained from regional proxy data. Soreq Cave speleothem data suggest that Δ_{T_a} was roughly between -8 and -10 °C in the Levant (Matthews et al., 2000; McGarry et al., 2004; Affek et al., 2008). Conversely, a Δ_{T_a} range of -2 to -6 °C with an extreme of -9 °C can be estimated from glacial coolings of 1 to 4 °C (Hayes et al., 2005) and 3 to 4 °C with a maximum of 5 to 6 °C (Arz et al., 2003) in nearby eastern Mediterranean and northern Red Sea surface waters, respectively (allowing that land temperature changes on average are about 1.5 × larger than marine temperature changes). Combined, these results suggest a range of potential Δ_{T_a} values of -2 to -10 °C, with most likely values in the region of -6 to -9 °C. Hence, the present study uses $\Delta_{T_a} = -7.5$ °C for the main assessment, and subsequently considers the sensitivity of the solution to a range between -6 and -9 °C. Finally, values for r differ strongly between studies, but were assessed and organised by the Dead Sea Research Team (2011) as: "*the relative humidity over the Dead Sea varies between 25% to 65%; however, these extreme values are infrequent, and 95% of the relative humidity is between 33% and 52%.*" Hence, the present study uses $r = 0.4$ for the main assessment, and

1. Set T_a, Δ_{Ta}/Δ_{Ts} (and so T_s), V, and r as discussed in text.

2. Calculate E_{lowS} (eq. 1).

3. Initialise using $H = 0$; $S = 330$; $\varepsilon = 1$; $\eta = 1$; $\alpha = 0.505$. Use $\Psi_t = (1 + f)\, F_\Psi \Psi_{mod}$ (see text). Set a seed-value for F_Ψ (e.g., 4). Run model 7000 y through step 4 to stabilise (generally needs only 1000 y).

4. For 'real' conditions after initalisation, iterate through entire record 10 times (≥ 3 is enough):

$$\Delta_{H(t)} = E_{net(t-1)}\, \Delta t$$
$$H_t = H_{t-1} + \Delta_{H(t)}$$
$$\varepsilon_t = 1.25 + 0.025\, H_t$$
$$\eta_t = 1 + 0.5\, \varepsilon_t H_t/118$$
$$S_t = S_{t-1}\, \eta_{t-1}/\eta_t$$
$$\alpha_t = 1 - 0.015\, S_t$$
$$E_t = \alpha_t\, E_{lowS(t)}$$
$$E_{net(t)} = E_{t-1} + \Psi_{t-1}\, 40/\varepsilon_t$$

5. Repeat steps 3 & 4 N times, changing F_Ψ each time so $F_{\Psi(n)} = F_{\Psi(n-1)}\, 200/(H_{max} - H_{mod})_{n-1}$, to optimise the solution toward H_{max} = +200 m (generally $N = 4$ is sufficient).

6. Find solutions for $t = i$, the time at which the maximum highstand of the glacial cycle (H_{max}) is achieved*:

$$\Delta_{E(i)} = E_i - E_{mod}$$
$$\Delta_{ElowS(i)} = E_{lowS(i)} - E_{lowS(mod)}$$
$$\Delta_{\Psi(i)} = \Psi_i - \Psi_{mod}$$
$$\Delta_{P(i)} = \Delta_{\Psi(t)} - \{\varepsilon_i\, \Delta_{E(i)} + (40 - \varepsilon_i)\, \Delta_{ElowS(i)}\}/40$$
$$P_i = \Delta_{P(i)} + P_{mod}$$

*(My solutions use a fixed value so i = 74100 y BP).

Fig. 2. Sequence of procedures and calculations followed in the model for Lake Lisan level reconstructions, as presented in this study.

subsequently considers the sensitivity of the solution to a range of r between 0.3 and 0.5.

Propagation of uncertainties assumes that total ranges for the various variables represent the equivalent of ±2 standard deviations (spanning about 95% of possible values), and chooses all parameters in such a way that extreme scenarios are formulated regardless of whether covariations between parameters might limit the range of possibilities in reality. The solutions then represent the ranges of precipitation change that would be coherent with evaporation assessments based on the controlling climate parameters, and lake-level change that would be coherent with reconstructions from the Lake Lisan sedimentary record. Finally, the field of solutions is compared with evidence from other reconstructions, to help characterise the most likely environmental changes over the region.

3. Results

Solutions to the main assessment, with $T_{a(mod)} = 26$ °C, $T_{s(mod)} = 28$ °C, $V_{mod} = 4$ m s^{-1}, $r = 0.4$ (mean estimates based on: Alpert et al., 1997; Hecht and Gertman, 2003; Dead Sea Research Team, 2011), $\Delta_V = 1.1$ m s^{-1} (see below for this value), and $\Delta_{T_a} = -7.5$°C, estimate values of $E_{mod} = -1.32$ m y^{-1}, $P_{mod} = 110$ mm y^{-1}, and $S_{mod} = 277$. Those values are very close to observations for times before major diversion of the Jordan River, as summarised before. Records through the last glacial cycle, as calculated within the main assessment, are shown in Fig. 3. For clarity, Fig. 3 shows all records after application of a rectangular 200-y smoothing window. The model produces (200-y smoothed) variations in the rates of lake-level change between extremes of about −1 and 1 m y^{-1}, with most of the variability restricted between −0.2 and 0.2 m y^{-1}. Salinities vary between 50 during lake-level highstands at times of cold glacial conditions and 350 during the peak warmth of the early to middle Holocene. There is a clear relationship between lake-level fluctuations and the imposed climatic fluctuations, which seems almost instantaneously/in phase on the scale plotted in Fig. 3. A magnified view of the variability between 60,000 and 45,000 years ago (Fig. 4) reveals that, more precisely, the strong hydrological fluxes caused by the imposed climatic variations lead to an in-phase response of the modelled rates of lake-level change, and that the resultant lake-level record is almost a century delayed relative to the climatic variations.

Lithological observations of change (e.g., Bartov et al., 2003, and its latest version as compiled in Torfstein et al., 2013a) suggest a more smoothed response of lake level than the model (blue line in Fig. 3), as well as a pronounced response to Heinrich Events, which will be explored later. There are several potential explanations for this difference between the model-inferred and observed responses. First it should be noted that the lithological record in the Holocene denotes very rapid variability. Hence, it is not likely that the lack of reported short-term variability in parts of the glacial cycle would have arisen because the system could not respond quick enough. In other words, the strong Holocene variability argues against the existence of long-term smoothing processes in the development of Lake Lisan's sedimentary record, which might have obscured more rapid lake-level variations. Moreover, a new interpretation of the pre-Holocene part of the record (pink line in Fig. 3, also after Torfstein et al., 2013a) begins to reveal much more fast, large-amplitude variability as well. Such developments in the observational record suggest that more information about pre-Holocene variability may still remain to be obtained from continued detailed field studies in this intriguing region. However, it is (at least) equally likely that there is a flaw in the present model's simplification that all crucial regional climate conditions (wind speed, temperature, and net precipitation) exactly covaried with the Greenland oxygen isotope record. Finally, there are intervals with signal amplitude similarity but slight temporal offsets between the observations (pink line) and the present Greenland-based simulation (black line) in Fig. 3, which may imply that some of the discrepancies simply reflect chronological uncertainties between the Lake Lisan record and the Greenland ice-core record. All of these suggestions represent interesting avenues for further development, for example using variation of climatic control parameters according to a regional climate model, and incorporating a model for sedimentation tied to the Lake Lisan level model. Unfortunately, little additional insight can be obtained from stable oxygen isotope records from Lake Lisan, because those predominantly reflect changes in the composition of eastern Mediterranean source waters (Kolodny et al., 2005). The latter in turn depend on global sea-level changes and superimposed surface-water dilution events due to African monsoon discharge (Grant et al., 2012).

The fine-scale offsets between model results and observations might be 'tuned' away by inverting the calculations (i.e., determining climate variations as a function of the exactly observed lake-level record), but this becomes somewhat circular before additional proxy support can be found to independently constrain the range of possible solutions and their uncertainties. Instead, I here accept that the current model output does not give a perfect fit with the observations, while noting that there is sufficient agreement in the larger-scale patterns to warrant further assessment of the propagation of uncertainties and sensitivities through the model to identify the major parameter ranges within which reasonable solutions exist.

The main assessment outlined above concerns a narrow set of values for the climatic control parameters. Therefore, the maximum

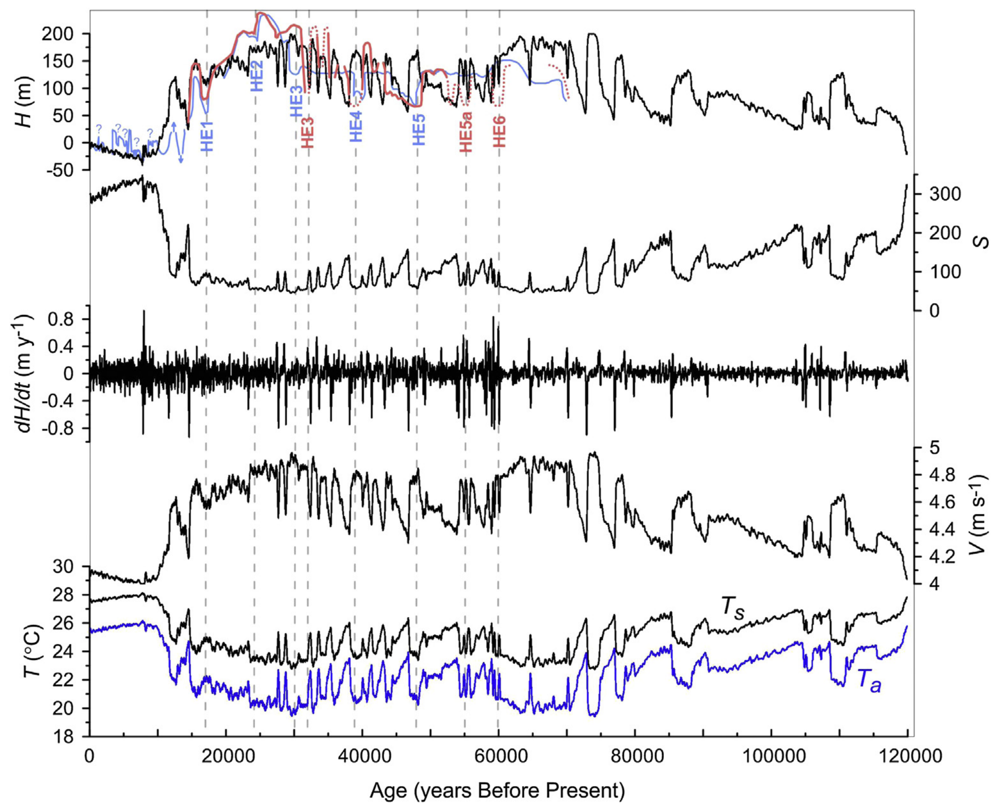

Fig. 3. Results for the model's main assessment outlined in the text. From bottom to top: the three key input records T_a, T_s, and V; and the reconstructed rates of lake-level change, salinities, and lake-levels. The light blue line in the upper panel represents lake-level variations inferred from observations, as compiled from previous work by ; see references therein). The pink line with more highly resolved variability represents a new interpretation by Torfstein et al. (2013a), which draws upon the lake-level reconstructions of Torfstein et al. (2013b). Blue and pink HE codes indicate lake level drops that were associated with Heinrich Events in the source publications. All model-based lines have been smoothed with a rectangular 200-y window, for clarity. (For interpretation of the references to colour in this figure legend, the reader is referred to the web version of this article.)

amplitude changes in the main assessment are evaluated as a function of the aforementioned ranges for control parameters $\Delta_{T_a}/\Delta_{T_s}$ and Δ_V (Fig. 5). The panels in Fig. 5 are related according to $E = E_{\mathrm{mod}} + \Delta_E$ and $P = P_{\mathrm{mod}} + \Delta_P$. The first observation from Fig. 5 is that the slopes of the contours clearly identify high sensitivity of the solutions to wind speed (through its impact on evaporation), which thus appears to be the dominant environmental control parameter involved in temporal changes in the regional

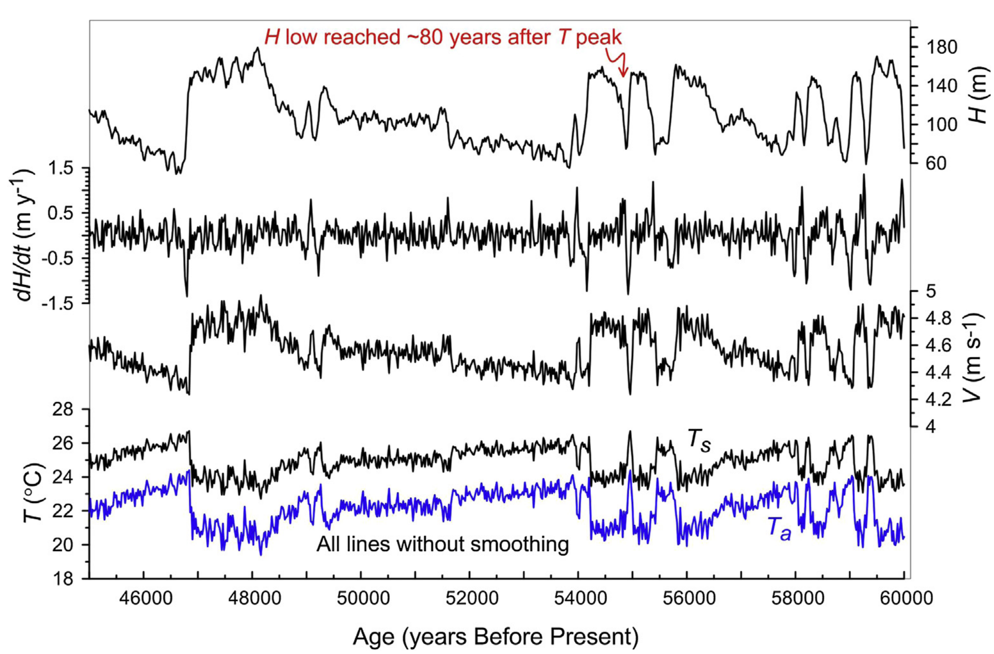

Fig. 4. As Fig. 3, but without salinity and zoomed in on the interval from 60,000 to 45,000 years ago. No smoothing has been applied.

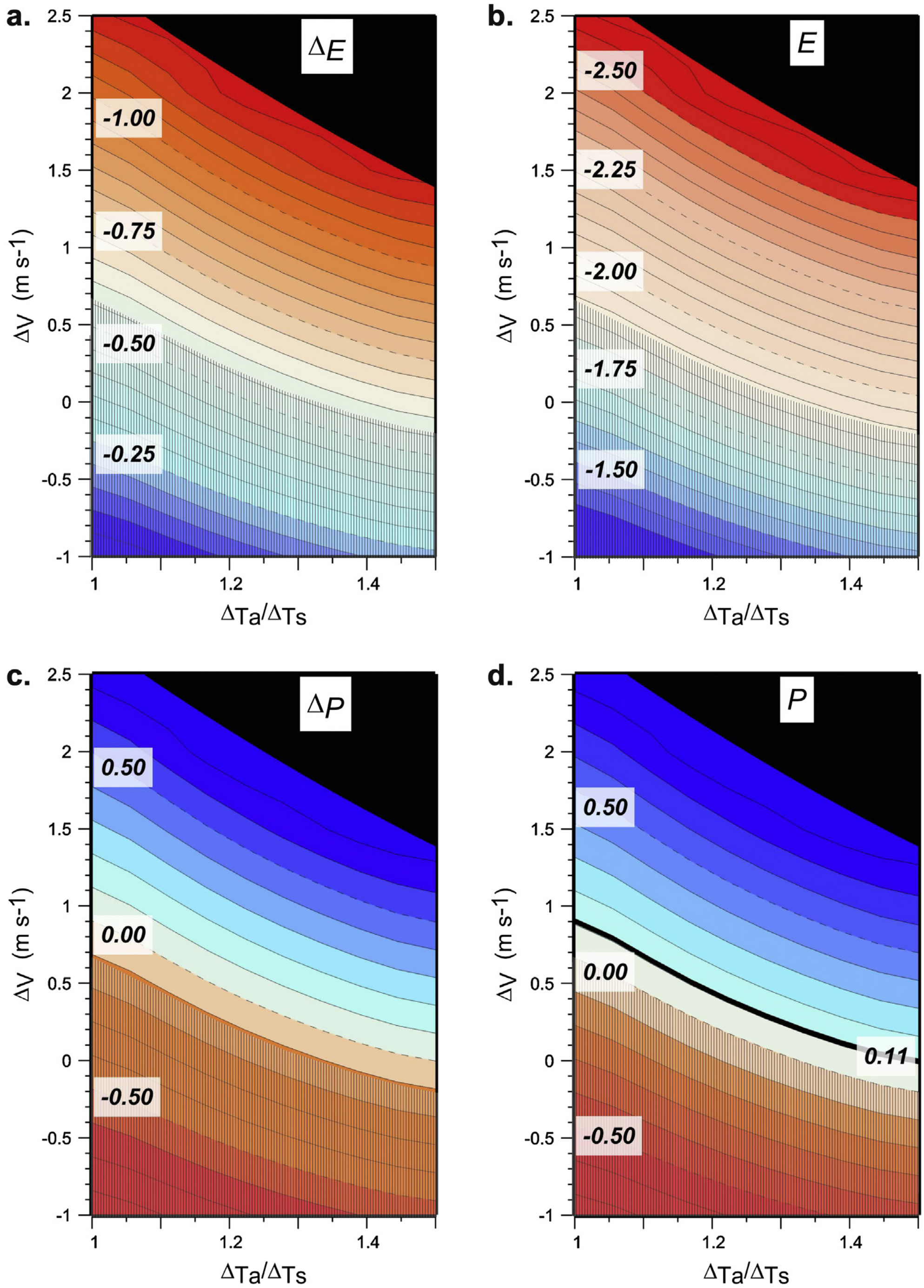

Fig. 5. Dependence of the solution for $H_{max} = +200$ m from the main assessment to realistic ranges for the critical control parameters $\Delta_{T_a}/\Delta_{T_s}$ and Δ_V, as outlined in the text. Blacked-out and grey hatched zones are explained in the 'results' section. All panels show contour values in m y^{-1}. Bold line indicates no change relative to the present.

hydrological budget. The second observation is that there are two 'special' zones in the graphs of Fig. 5. First is the blacked-out, top-right corner, which marks a field where evaporation rates are so high that there are no solutions for which lake level achieves a maximum of +200 m (to understand this, note that changing evaporation rates also affect *net* precipitation over the catchment). Second is the hatched bottom field in the graphs, where calculated rates of mean precipitation are negative (see panel d). Although mathematically possible ('negative precipitation' simply being an additional evaporation term), this condition is unrealistic in the real world; it would require lake water to be advected upslope away from the lake into the wider catchment in order to there sustain the 'negative precipitation'/evaporative loss.

There are further arguments against the plausibility of the hatched bottom field. Stable oxygen isotope calculations suggest that glacial winds may have strengthened over the Red Sea (Rohling, 1994) and were constant or slightly stronger over the eastern Mediterranean, relative to the present (Rohling, 1999). Enzel et al. (2003, 2008) and Frumkin et al. (2011) also suggested that any precipitation increase over the Levant during the last glacial would have been related to enhanced intensity/frequency of Cyprus Lows, which would lead to increased mean wind speeds.

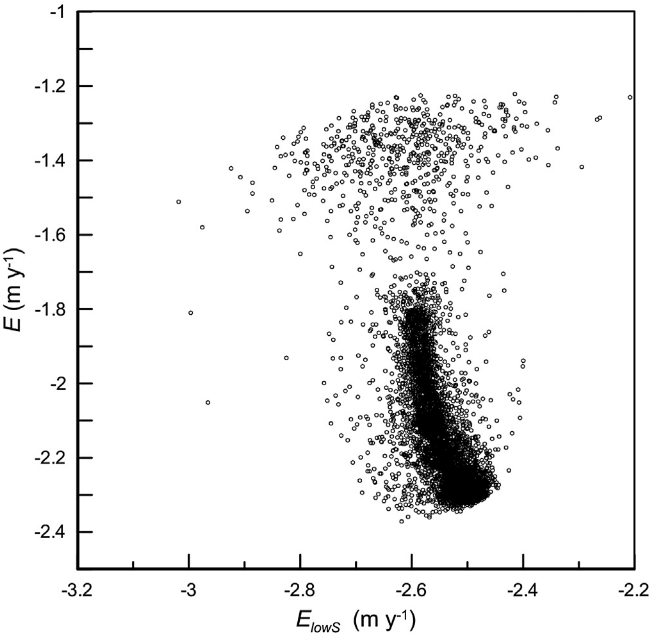

Fig. 6. Comparison, for each age-point in the record, between the 'pan evaporation' value (E_{lowS}) calculated with Equation (1), and the salinity-adjusted evaporation rate from Lake Lisan ($E = \alpha E_{lowS}$).

Hence, solutions at $\Delta_V \leq 0$ m s^{-1} are less plausible than those at $\Delta_V > 0$ m s^{-1}.

In the window of plausible solutions for the main assessment (in between the grey-hatched and blacked-out fields in Fig. 5), reconstructed evaporation rates from Lake Lisan during peak glacial highstands at around +200 m are $-2.62 < E < -1.88$ m y^{-1}, with mean precipitation rates over the wider catchment at $0 < P < 860$ mm y^{-1}. The stronger evaporation rates at that time compared to E_{mod} (-1.3 m y^{-1}) are predominantly due to reduced salinity during times of increased lake level/volume (through α). The impact of the salinity effect cannot be emphasised enough; the results from this study should *not* be taken to imply that regional pan evaporation rates (E_{lowS}) were strongly increased during glacial times. Instead, pan evaporation rates in the main assessment were only slightly increased at glacial times, and largely remained between -2.8 and -2.4 m y^{-1} throughout the modelled time-series (toward the lower end during cold stadials, and toward the higher end during the warmest episodes) (Fig. 6). Clearly, the climatological controls on evaporation rate from Lake Lisan were secondary to the salinity control. Because the salinity effect causes an increase in evaporative loss from Lake Lisan as its level rises, and a reduction in the evaporative loss as lake level drops, the salinity effect represents a powerful negative feedback process to the primary, climatically imposed changes in lake level.

Here, it is interesting to note that moisture availability to soils/vegetation and for cave speleothem growth in the area is affected by the always-high pan evaporation rates (E_{lowS}) (Fig. 6). However, regional precipitation rates are so low that even relatively minor variations in E_{lowS}, over a range of up to 0.4 m y^{-1}, would equal the impact of 300–400% changes in regional precipitation. Given that vegetation/soil water availability (and groundwater recharge) are functions of the net freshwater budget of the study region, a simple fluctuation of evaporation might thus produce a change in vegetation (or speleothem growth) that could be misconstrued as a doubling or more of precipitation. It is evident that reconciliation of vegetation-and/or speleothem-inferred 'humidity' with lake levels is a non-trivial exercise, especially if the lake is a saline lake, like Lake Lisan.

The reconstructed fields of Fig. 5 may be compared with values that have been proposed in the literature based on other data. First, geochemical calculations of the inorganic carbon budget of Lake Lisan have been used to suggest a roughly 5-fold higher inorganic carbon influx into the lake during glacial times than during the Holocene (Barkan et al., 2001). Under a simple assumption of proportionality, this suggests a 5-fold increase in mean precipitation over the wider catchment area; i.e., $P \approx 5P_{mod} \approx 550$ mm y^{-1}. Speleothem evidence from the western margin of the Dead Sea has also been used to suggest that glacial precipitation rates reached 500 mm y^{-1} or more (e.g., Enzel et al., 2008; Frumkin et al., 2011), although this may be subject to caveats discussed in the previous paragraph. The two independent methods are in good agreement, which instills confidence in an estimate of $P \approx 500$ mm y^{-1}. To

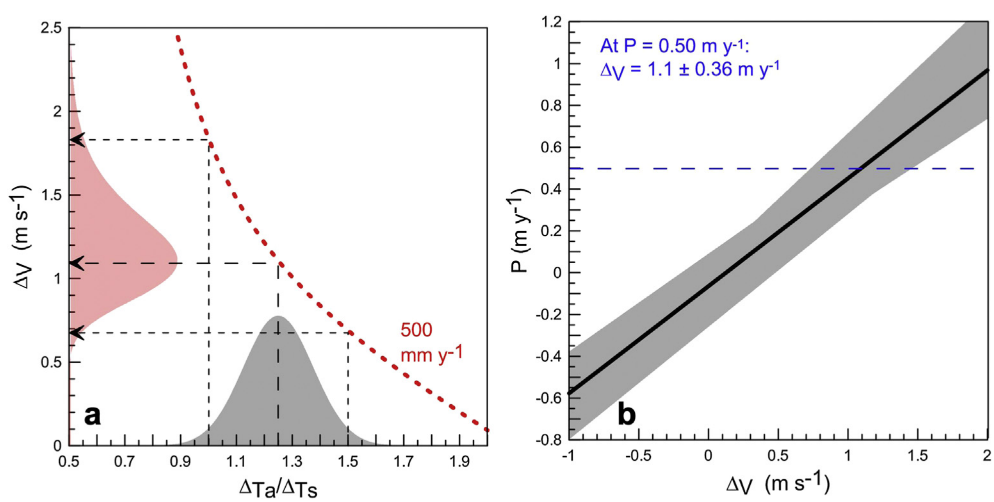

Fig. 7. Assessment of uncertainties in the main solution. **a**. Illustration, for the main solution at $P = 500$ mm y^{-1}, of the implications of uncertainty in the ratio $\Delta_{T_a}/\Delta_{T_s}$ for the inferred Δ_V values. Uncertainty in $\Delta_{T_a}/\Delta_{T_s}$ is captured along the *X*-axis using a normal distribution with 95% probability within the bounds of 1.0–1.5 (peak of the probability curve is set to an arbitrary level for clearest illustration). Projection of the $\Delta_{T_a}/\Delta_{T_s}$ probability distribution onto the model solution gives the probability distribution for Δ_V along the *Y*-axis, which becomes clearly skewed with an extended tail to high values. Dashed lines connect probability maxima and 95% confidence limits. **b**. Illustration of additional uncertainty in Δ_V due to 2σ (95%) equivalent uncertainties in r (= 0.4 ± 0.1) and Δ_{T_a} (= −7.5 ± 1.5 °C). Root mean square addition of uncertainties from **a** and **b** gives $\Delta_V = 1.10^{+0.81}/_{-0.55}$ m s^{-1} (95% probability).

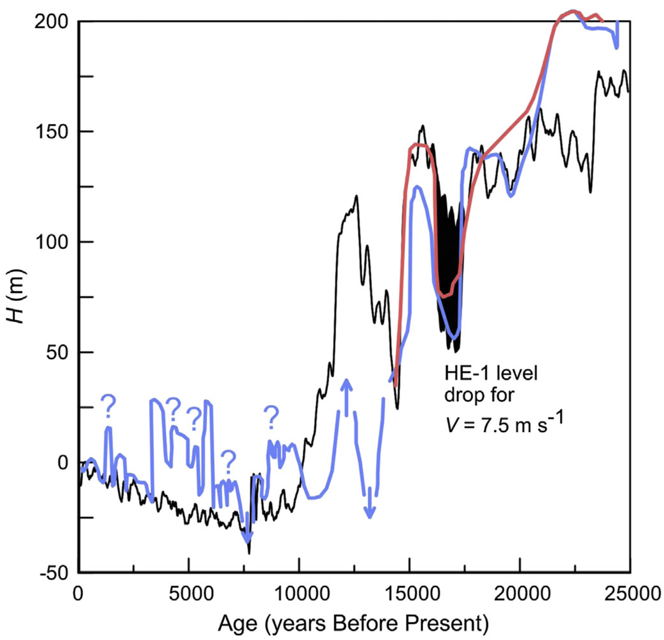

Fig. 8. Illustration of the drop in lake level at the time of Heinrich Event 1 that results from manual overriding of the main assessment's inferred wind-speed values in that interval by a high value of 7.5 m s^{-1}. Model lines have been smoothed with a rectangular 200-y window to avoid clutter. The light blue line represents lake-level variations inferred from previous observations, as compiled in Torfstein et al. (2013a; see also light blue line in Fig. 3). The pink line represents a new interpretation by Torfstein et al. (2013a), which draws upon the lake-level reconstructions of Torfstein et al. (2013b). (For interpretation of the references to colour in this figure legend, the reader is referred to the web version of this article.)

assess the implications of this estimate, the 500 mm y^{-1} contour from Fig. 5d is singled out in Fig. 7a. Next, a normal distribution is formulated for $\Delta_{T_a}/\Delta_{T_s}$ using a mean of 1.25 and a 2σ (95% probability) window of ±0.25, based on the range arguments presented before. This normal distribution is projected onto the $P = 500$ mm y^{-1} line to derive the corresponding estimates for Δ_V, which gives $\Delta_V = 1.10\ ^{+0.73}/_{-0.42}$ m s^{-1} (95% probability).

In addition to the uncertainties already accounted for, the inferred probabilities for glacial Δ_V during peak lake-level highstands also depend on uncertainties in r and Δ_{T_a}. In other words, realistic ranges of r and Δ_{T_a} need to be accounted for; as discussed above, these amount to $r = 0.4 \pm 0.1$ and $\Delta_{T_a} = -7.5 \pm 1.5$°C (2$\sigma$ equivalent). These ranges produce extra uncertainty in the inferred values of Δ_V that amounts to ±0.36 m s^{-1} (Fig. 7b). Root mean square addition gives a final estimate for glacial Δ_V, namely $\Delta_V = 1.10\ ^{+0.81}/_{-0.55}$ m s^{-1} (95% probability). The observations of Lake Lisan levels up to 200 m above the Dead Sea level, along with $P = 500$ mm y^{-1}, are therefore found to be quantitatively consistent if glacial wind speeds were significantly (beyond 95% uncertainty) increased relative to their present-day mean value of about 4 m s^{-1}.

Finally, the model provides insight into the sharp drops in Lake Lisan level that have been reported for the coldest millennial-scale events during the last glacial cycle that coincided with North Atlantic Heinrich Events (Bartov et al., 2003; Torfstein et al., 2013a,b). These contrast sharply with the 'normal' pattern of high lake levels during cold periods. Fig. 5d illustrates that, close to (but not inside) the blacked-out zone, a given period of time with relatively high wind speeds and/or high $\Delta_{T_a}/\Delta_{T_s}$ ratios may be marked by high lake levels, as long as precipitation rates were high. However, if (predominantly) windspeed were to increase further, then the solution would shift into the blacked-out zone. In that zone, evaporation rates are so large that lake levels drop sharply, regardless of high precipitation rates. To evaluate the potential impacts, the main assessment's inferred record of V has been adapted by manually replacing its values of about 4.6 m s^{-1} in the interval of Heinrich Event 1 (taken as 17,450–16,250 years ago to match the timing of the observed lake-level drop) by values of 7.5 m s^{-1} (i.e., $\Delta_{V(HE1)} = 3.5$ m s^{-1}) and subsequently calculated lake levels are compared with the main assessment (Fig. 8). Although this simply imposed, large change represents an artificial experiment, it clearly highlights exceptional wind speeds as a key candidate process for explaining the observed lake-level drops during Heinrich Events.

4. Conclusions

Although the full intricacies of D–O scale variability in Lake Lisan level are not yet reproduced with the model as is, it already demonstrates that increased windiness (and thus evaporation) must have been an important component of environmental changes around Lake Lisan if realistic bounds on precipitation increase are considered from the compiled data. For glacial rainfall reaching 500 mm y^{-1}, a value inferred from the literature (Enzel et al., 2008; Frumkin et al., 2011), the estimated increase in mean wind speed is 0.6–1.9 m s^{-1} (95% probability). Wind-speed increase over the region is consistent with the development of glacial windblown dust (loess) deposits along the northern Negev Desert margin (Enzel et al., 2008).

The results support a notable increase in (winter) storminess that caused both precipitation and increased winds, as was qualitatively suggested before from geological and geomorphological evidence (Enzel et al., 2003, 2008; Frumkin et al., 2011). The present study therefore provides quantitative support for their proposed mechanism of a stronger west-east "*funneling of Mediterranean cyclones into the central Levant, replacing the moister and semi-arid Mediterranean zone with a wetter temperate climate.*" This mechanism also is consistent with evidence of enhanced atmospheric instability over the central Mediterranean during glacial times, with intensified formation of Mediterranean depressions due to cold polar/continental air outbursts through gaps in the mountain ranges to the north of the basin (Kuhlemann et al., 2008).

During Heinrich Events, which were marked by regional cooling, the level of Lake Lisan dropped sharply (Bartov et al., 2003; Torfstein et al., 2013a,b), in contrast with the 'normal' association between cold conditions and high lake levels during the last glacial cycle. The present study identifies exceptional wind speeds as a key candidate process for explaining these drops at times of Heinrich Events. Distinct increases in wind speed at times of Heinrich Events agree with other proxy evidence from the Mediterranean and Red Sea region (e.g., Rohling et al., 1998; Moreno et al., 2002; Larrasoaña et al., 2003; Enzel et al., 2008; Roberts et al., 2011).

Acknowledgements

I thank M. Stein, S. Goldstein, Y. Enzel, and M. Bar-Matthews for sharing their extensive knowledge and insights during the Ein Gedi fieldtrip of the Kaplan Conference in March 2012, and A.P. Roberts, K. Grant, and two anonymous reviewers for comments on earlier drafts. This study contributes to UK Natural Environment Research Council projects NE/E01531X/1 (RESET), NE/I009906/1 (iGlass), and NE/H004424/1, to a Royal Society-Wolfson Research Merit Award, and to Australian Laureate Fellowship FL120100050.

Appendix I. Key parameters used in the calculations.

A	area of Lake Lisan
A_{catch}	area of catchment basin

A_{DSmod} area of modern Dead Sea. Note: areas are all non-dimensionalised using A_{DSmod}
E_{lowS} "pan evaporation" rate from low-salinity water (from Equation 1)
α factor for salinity impact on E, where $\alpha = 1-0.015\ S$
S Lake Lisan salinity (calculated by volumetric dilution)
E evaporation from Lake Lisan ($E = \alpha E_{lowS}$)
E_{mod} modern value of E (calculated; equal to -1.3 m y^{-1} in main assessment)
H level of Lake Lisan relative to southern Dead Sea threshold 10 m above current Dead Sea level
P mean gross precipitation over catchment basin (corrected for evapotranspiration)
P_{mod} modern value of P (calculated; equal to 110 mm y^{-1} in main assessment)
r relative humidity (0.4 ± 0.1 at 2σ)
T_a mean air temperature ($T_a = T_{a(mod)} + f\Delta_{T_a}$)
$T_{a(mod)}$ modern value of T_a (26 °C)
Δ_{T_a} variation in T_a relative to $T_{a(mod)}$ (peak of -7.5 ± 1.5 °C at 2σ, using Δ_{T_a} variability that follows NGRIP climate variability)
T_s mean surface-water temperature ($T_s = T_{s(mod)} + f\Delta_{T_s}$)
$T_{s(mod)}$ modern value of T_s (28 °C)
Δ_{T_s} defined using Δ_{T_a} variability that follows NGRIP climate variability, within a range of $1.0 \le \Delta_{T_a}/\Delta_{T_s} \le 1.5$
V mean wind speed ($V = V_{mod} + \Delta_V$)
V_{mod} modern value of V (4 m s^{-1})
Δ_V past change of wind speed relative to V_{mod}, with a variability that follows NGRIP climate changes
Ψ mean *net* precipitation over catchment basin (before correction for influences of evapotranspiration)
Ψ_{mod} modern value of Ψ (calculated; equal to 33 mm y^{-1} in main assessment)
Ω volume of Lake Lisan
Ω_{DSmod} volume of modern Dead Sea. Note: volume change calculations are based on non-dimensionalised lake area and non-dimensionalised depth (the latter using a present-day mean Dead Sea depth of 118 m)

References

Abbate, E., Sagri, M., 2012. Early to Middle Pleistocene Homo dispersals from Africa to Eurasia: geological, climatic and environmental constraints. Quaternary International 267, 3–19.
Abbott, P.F., Tabony, R.C., 1985. The estimation of humidity parameters. Meteorological Magazine 114, 49–56.
Affek, H., Bar-Matthews, M., Ayalon, A., Matthews, A., Eiler, J.M., 2008. Glacial/interglacial temperature variations in Soreq cave speleothems as recorded by 'clumped isotope' thermometry. Geochimica et Cosmochimica Acta 72, 5351–5360.
Alpert, P., Shafir, H., Issahary, D., 1997. Recent changes in the climate at the Dead Sea – a preliminary study. Climatic Change 37, 513–537.
Arz, H.W., Pätzold, J., Müller, P.J., Moammar, M.O., 2003. Influence of Northern Hemisphere climate and global sea level rise on the restricted Red Sea marine environment during termination I. Paleoceanography 18, 1053. http://dx.doi.org/10.1029/2002PA000864.
Asmar, B.N., Ergenzinger, P., 2002a. Environmental effects of the Dead Sea–Red Sea canal. International Journal of Environmental Studies 59, 647–664.
Asmar, B.N., Ergenzinger, P., 2002b. Prediction of the Dead Sea dynamic behaviour with the Dead Sea–Red Sea canal. Advances in Water Resources 25, 783–791.
Asmar, B.N., Ergenzinger, P., 2002c. Dynamic simulation of the Dead Sea. Advances in Water Resources 25, 263–277.
Asmar, B.N., Ergenzinger, P., 2002d. Long-term prediction of the water level and salinity in the Dead Sea. Hydrological Processes 16, 2819–2831.
Asmar, B.N., Ergenzinger, P., 2003. Effect of the Dead Sea–Red Sea canal modelling on the prediction of the Dead Sea conditions. Hydrological Processes 17, 1607–1621.
Barkan, E., Luz, B., Lazar, B., 2001. Dynamics of the carbon dioxide system in the Dead Sea. Geochimica et Cosmochimica Acta 65, 355–368.
Bartov, Y., Stein, M., Enzel, Y., Agnon, A., Reches, Z., 2002. Lake levels and sequence stratigraphy of Lake Lisan, the Late Pleistocene precursor of the Dead Sea. Quaternary Research 57, 9–21.
Bartov, Y., Goldstein, S.L., Stein, M., Enzel, Y., 2003. Catastrophic arid episodes in the east Mediterranean linked with the Atlantic Heinrich events. Geology 31, 439–442.
Braconnot, P., Otto-Bliesner, B., Harrison, S., Joussaume, S., Peterschmitt, J.Y., Abe-Ouchi, A., Crucifix, M., Driesschaert, E., Fichefet, Th., Hewitt, C.D., Kageyama, M., Kitoh, A., Laîné, A., Loutre, M.F., Marti, O., Merkel, U., Ramstein, G., Valdes, P., Weber, S.L., Yu, Y., Zhao, Y., 2007. Results of PMIP2 coupled simulations of the mid-Holocene and Last Glacial Maximum – Part 1: experiments and large-scale features. Climate of the Past 3, 261–277.
Braconnot, P., Harrison, S.P., Kageyama, M., Bartlein, P.J., Masson-Delmotte, V., Abe-Ouchi, A., Otto-Bliesner, B., Zhao, Y., 2012. Evaluation of climate models using palaeoclimate data. Nature Climate Change 2, 417–424.
Cacho, I., Grimalt, J.O., Canals, M., 2002. Response of the Western Mediterranean Sea to rapid climatic variability during the last 50,000 years: a molecular biomarker approach. Journal of Marine Systems 33–34, 253–272.
Cacho, I., Grimalt, J.O., Canals, M., Sbaffi, L., Shackleton, N.J., Schönfeld, J., Zahn, R., 2001. Variability of the western Mediterranean Sea surface temperatures during the last 25,000 years and its connection with the northern hemisphere climatic changes. Paleoceanography 16, 40–52.
Cacho, I., Grimalt, J.O., Pelejero, C., Canals, M., Sierro, F.J., Flores, J.A., Shackleton, N.J., 1999. Dansgaard–Oeschger and Heinrich event imprints in Alboran Sea paleotemperatures. Paleoceanography 14, 698–705.
Dansgaard, W., Johnsen, S.J., Clausen, H.B., Dahl-Jensen, D., Gundestrup, N.S., Hammer, C.U., Hvidberg, C.S., Steffensen, J.P., Sveinbjornsdottir, A.E., Jouzel, J., Bond, G., 1993. Evidence for general instability of past climate from a 250 kyr ice core. Nature 364, 218–219.
Dead Sea Research Team, 2011. Red Sea–Dead Sea Water Conveyance Study Program: Dead Sea Study, Mid-term Report, Revised (April 2011), p. 84. (GSI Report Number: GSI/24/2010. TAHAL Report Number: IL-201280-R10-055A).
Enzel, Y., Amit, R., Dayan, U., Crouvi, O., Kahana, R., Ziv, B., Sharon, D., 2008. The climatic and physiographic controls of the eastern Mediterranean over the late Pleistocene climates in the southern Levant and its neighboring deserts. Global Planetary Change 60, 165–192.
Enzel, Y., Bookman (Ken-Tor), R., Sharon, D., Gvirtzman, H., Dayan, U., Ziv, B., Stein, M., 2003. Late Holocene climates of the Near East deduced from Dead Sea level variations and modern regional winter rainfall. Quaternary Research 60, 263–273.
FAO GEONETWORK, 2010. Hydrological Basins in Near East (Derived From HydroSHEDS). http://www.fao.org/geonetwork/srv/en/metadata.show?currTab=simple&id=37299# (accessed August 2012).
Fernandes, C.A., Rohling, E.J., Siddall, M., 2006. Absence of post-Miocene Red Sea land bridges: biogeographic implications. Journal of Biogeography 33, 961–966.
Frigola, J., Moreno, A., Cacho, I., Canals, M., Sierro, F.J., Flores, J.A., Grimalt, J.O., 2008. Evidence of abrupt changes in Western Mediterranean Deep Water circulation during the last 50 kyr: a high-resolution marine record from the Balearic Sea. Quaternary International 181, 88–104.
Frumkin, A., Bar-Yosef, O., Schwarcz, H.P., 2011. Possible paleohydrologic and paleoclimatic effects on hominin migration and occupation of the Levantine Middle Paleolithic. Journal of Human Evolution 60, 437–451.
Garrett, C., Outerbridge, R., Thompson, K., 1993. Interannual variability in Mediterranean heat budget and buoyancy fluxes. Journal of Climate 6, 900–910.
Grant, K.M., Rohling, E.J., Bar-Matthews, M., Ayalon, A., Medina-Elizalde, M., Bronk Ramsey, C., Satow, C., Roberts, A.P., 2012. Rapid coupling between ice volume and polar temperature over the past 150 kyr. Nature 491, 744–747.
Grootes, P.M., Stuiver, M., White, J.W.C., Johnsen, S., Jouzel, J., 1993. Comparison of oxygen isotope records from the GISP2 and GRIP Greenland ice cores. Nature 366, 552–554.
Hayes, A., Kucera, M., Kallel, N., Sbaffi, L., Rohling, E.J., 2005. Glacial Mediterranean Sea surface temperatures reconstructed from planktonic foraminiferal assemblages. Quaternary Science Reviews 24, 999–1016.
Hecht, A., Gertman, I., 2003. Dead Sea meteorological climate. In: Nevo, E., Oren, A., Wasser, S.P. (Eds.), Biodiversity of Cyanoprocaryotes, Algae and Fungi of Israel; Fungal Life in the Dead Sea. International Center for Cryptogamic Plants and Fungi, Institute of Evolution, University of Haifa, Israel, p. 361.
Kolodny, Y., Stein, M., Machlus, M., 2005. Sea-rain-lake relation in the Last Glacial East Mediterranean revealed by $\delta^{18}O-\delta^{13}C$ in Lake Lisan aragonites. Geochimica et Cosmochimica Acta 69, 4045–4060.
Kuhlemann, J., Rohling, E.J., Kumrei, I., Kubik, P., Ivy-Ochs, S., Kucera, M., 2008. Regional synthesis of Mediterranean atmospheric circulation during the Last Glacial Maximum. Science 321, 1338–1340.
Larrasoaña, J.C., Roberts, A.P., Rohling, E.J., Winklhofer, M., Wehausen, R., 2003. Three million years of monsoon variability over the northern Sahara. Climate Dynamics 21, 689–698.
Lensky, N.G., Dvorkin, Y., Lyakhovsky, V., Gertman, I., Gavrieli, I., 2005. Water, salt, and energy balances of the Dead Sea. Water Resources Research 41, W12418. http://dx.doi.org/10.1029/2005WR004084.
Lisker, S., Vaks, A., Bar-Matthews, M., Porat, R., Frumkin, A., 2009. Stromatolites in caves of the Dead Sea Fault Escarpment: implications to latest Pleistocene lake levels and tectonic subsidence. Quaternary Science Reviews 28, 80–92.
Magal, E., Weisbrod, N., Yakirevich, A., Kurtzman, D., Yechieli, Y., 2010. Line-source multi-tracer test for assessing high groundwater velocity. Ground Water 48, 892–897.
Martrat, B., Grimalt, J.O., Lopez-Martinez, C., Cacho, I., Sierro, F.J., Flores, J.A., Zahn, R., Canals, M., Curtis, J.H., Hodell, D.A., 2004. Abrupt temperature

changes in the western Mediterranean over the past 250,000 years. Science 306, 1762–1765.
Martrat, B., Grimalt, J.O., Shackleton, N.J., de Abreu, L., Hutterli, M.A., Stocker, T.F., 2007. Four climate cycles of recurring deep and surface water destabilizations on the Iberian margin. Science 317, 502–507.
Matthews, A., Ayalon, A., Bar-Matthews, M., 2000. D/H ratios of fluid inclusions of Soreq cave (Israel) speleothems as a guide to the Eastern Mediterranean Meteoric Line relationships in the last 120 ky. Chemical Geology 166, 183–191.
McGarry, S., Bar-Matthews, M., Matthews, A., Vaks, A., Schilman, B., Ayalon, A., 2004. Constraints on hydrological and paleotemperature variations in the Eastern Mediterranean region in the last 140 ka given by the δD values of speleothem fluid inclusions. Quaternary Science Reviews 23, 919–934.
Migowski, C., Stein, M., Prasad, S., Negendank, J.F.W., Agnon, A., 2006. Holocene climate variability and cultural evolution in the Near East from the Dead Sea sedimentary record. Quaternary Research 66, 421–431.
Moreno, A., Cacho, I., Canals, M., Prins, M.A., Sánchez-Goñi, M.F., Grimalt, J.O., Weltje, G.J., 2002. Saharan dust transport and high-latitude glacial climatic variability: the Alboran Sea record. Quaternary Research 58, 318–328.
North Greenland Ice Core Project Members, 2004. High-resolution record of Northern Hemisphere climate extending into the last interglacial period. Nature 431, 147–151.
Prasad, S., Vos, H., Negendank, J.F.W., Waldmann, N., Goldstein, S.L., Stein, M., 2004. Evidence from Lake Lisan of solar influence on decadal- to centennial-scale climate variability during marine oxygen isotope stage 2. Geology 32, 581–584.
Roberts, A.P., Rohling, E.J., Grant, K.M., Larrasoaña, J.C., Liu, Q., 2011. Atmospheric dust variability from Arabia and China over the last 500,000 years. Quaternary Science Reviews 30, 3537–3541.
Rohling, E.J., 1994. Glacial conditions in the Red Sea. Paleoceanography 9, 653–660.
Rohling, E.J., 1999. Environmental controls on salinity and $\delta^{18}O$ in the Mediterranean. Paleoceanography 14, 706–715.
Rohling, E.J., Hayes, A., Kroon, D., De Rijk, S., Zachariasse, W.J., 1998. Abrupt cold spells in the NW Mediterranean. Paleoceanography 13, 316–322.
Salhotra, A.M., Adams, E.E., Harleman, D.R.F., 1985. Effect of salinity and ionic composition on evaporation: analysis of Dead Sea evaporation pans. Water Resources Research 21, 1336–1344.
Sprovieri, R., Di Stefano, E., Incarbona, A., Gargano, M.E., 2003. A high-resolution record of the last deglaciation in the Sicily Channel based on foraminifera and calcareous nannofossil quantitative distribution. Palaeogeography, Palaeoclimatology, Palaeoecology 202, 119–142.
Stanhill, G., 1994. Changes in the rate of evaporation from the Dead Sea. International Journal of Climatology 14, 465–471.
Stein, M., Goldstein, S.L., 2006. U–Th and radiocarbon chronologies of late Quaternary lacustrine records of the Dead Sea basin: methods and applications. In: Enzel, Y., Agnon, A., Stein, M. (Eds.), New Frontiers in Dead Sea Paleoenvironmental Research. GSA Special Paper, vol. 401. GSA, Boulder, GSA, pp. 33–51.
Torfstein, A., Haase-Schramm, A., Waldmann, N., Kolodny, Y., Stein, M., 2009. U-series and oxygen isotope chronology of the mid-Pleistocene Lake Amora (Dead Sea basin). Geochimica et Cosmochimica Acta 73, 2603–2630.
Torfstein, A., Goldstein, S.L., Kagan, E., Stein, M., 2013a. Integrated multi-site U–Th chronology of the last glacial Lake Lisan. Geochimica et Cosmochimica Acta 104, 210–231.
Torfstein, A., Goldstein, S.L., Stein, M., Enzel, Y., 2013b. Impacts of abrupt climate changes in the Levant from last glacial Dead Sea levels. Quaternary Science Reviews 69, 1–7.
Waldmann, N., Starinsky, A., Stein, M., 2007. Primary carbonates and Ca-chloride brines as monitors of a paleo-hydrological regime in the Dead Sea basin. Quaternary Science Reviews 26, 2219–2228.
Waldmann, N., Torfstein, A., Stein, M., 2010. Northward intrusions of low- and mid-latitude storms across the Saharo-Arabian belt during past interglacials. Geology 38, 567–570.
Watson, R.T., Zinyowera, M.C., Moss, R.H., Dokken, D.J., 1997. The Regional Impacts of Climate Change: an Assessment of Vulnerability. Special Report of IPCC Working Group II. Intergovernmental Panel on Climate Change, ISBN 92-9169-110-0, p. 27.
Wdowinski, S., Zilberman, E., 1997. Systematic analyses of the large-scale topography and structure across the Dead Sea rift. Tectonics 16, 409–424.
Wells, N.C., 1986. The Atmosphere and Ocean: a Physical Introduction. Taylor and Francis, Bristol, Pa, p. 347.
Wells, N.C., 1995. Surface heat fluxes in the western equatorial Pacific Ocean. Annales Geophysicae 13, 1047–1053.